High precision quantum control of single donor spins in Si

Rajib Rahman,[1] Cameron. J. Wellard,[2] Forrest R. Bradbury,[3] Marta
Prada,[1] Jared H. Cole,[2] Gerhard Klimeck,[1,4] and Lloyd C. L. Hollenberg[2]

[1]*Network for Computational Nanotechnology, Purdue University, West Lafayette, IN 47907, USA*
[2]*Center for Quantum Computer Technology, School of Physics, University of Melbourne, VIC 3010, Australia*
[3]*Department of Electrical Engineering, Princeton University, Princeton, NJ 08544, USA*
[4]*Jet Propulsion Laboratory, California Institute of Technology, Pasadena, CA 91109, USA*
(Dated: May 8, 2007)

The Stark shift of the hyperfine coupling constant is investigated for a P donor in Si far below the ionization regime in the presence of interfaces using Tight-binding and Band Minima Basis approaches and compared to the recent precision measurements. In contrast to previous effective mass based results, the quadratic Stark coefficient obtained from both theories agrees closely with the experiments. This work represents the most sensitive and precise comparison between theory and experiment for single donor spin control. It is also shown that there is a significant linear Stark effect for an impurity near the interface, whereas, far from the interface, the quadratic Stark effect dominates. Such precise control of single donor spin states is required particularly in quantum computing applications of single donor electronics, which forms the driving motivation of this work.

PACS numbers: 71.55.Cn, 03.67.Lx, 85.35.Gv, 71.70.Ej

Solid state quantum computer architectures have received considerable attention in recent years due to their promise of scalability and utilization of the vast knowledge and experience of the semiconductor fabrication industry. Several proposals employ the electronic states of phosphorus donors in silicon to encode qubits based on nuclear spin [1], electronic spin [2–4], or the electronic states of a singly ionized two-donor system [5]. Two-dimensional architectures for such qubits have been proposed to demonstrate scalability strategies [6].

In Kane's original nuclear spin qubit proposal [1], and the more recent semi-global control electron spin proposal [3], single-qubit operations are performed by electrically controlling the hyperfine interaction between the donor electron spin and the nuclear spin of the P impurity. To implement rigorous large-scale quantum algorithms protected by Quantum Error Correction (QEC), the donor wave function dependent hyperfine coupling constant needs to be controlled to a very high degree of precision. Recent experiments have made tremendous inroads towards achieving such control of donor spin. In Ref [7] coherent oscillations of P donor electron spins were measured by electrically detected magnetic resonance. Similar techniques were used in Ref [8] to invesitgate the hyperfine interaction in the presence of lattice strain for Si grown on $Si_{1-x}Ge_x$. This work is motivated by a recent ESR experiment [9] that measured the Stark shifts for ^{121}Sb donors in silicon buried at a depth of 150 nm from an interface. A quadratic dependence of the hyperfine coupling constant and electron g-factor on the electric field was reported far below the ionization regime. A weak linear Stark effect was also reported. In comparison with theory, effective mass theory (EMT) inferred from the work of Friesen [16] predicts a quadratic Stark shift some ten times greater than the measured re-

sult. This letter investigates the Stark shift in the experimentally probed regime well below the ionization threshold and shows that two sophisticated methods, namely Tight-Binding (TB) and Band Minima Basis (BMB), are able to predict the system control parameters in contrast with EMT. The Sb and P donors in Si can be treated as analogous because their ground state binding energies differ only by 2.8 meV, and their 1s manifold splittings due to valley-orbit coupling and local perturbations are also similar in nature [10]. This is important as both the TB and BMB methods employed here are optimized for P donors. This agreement between theory and experiment for a non-trivial measure of wave function control, by two distinct theoretical approaches, represents the most precise test of our understanding of donor systems. The current level of theoretical understanding of the system reported here, in conjunction with the advancement in single atom fabrication technologies [11] and the above-mentioned experiment, represents one of the first steps towards experimental realization of high precision control of donor spins in Si.

Most of the approaches based on EMT have involved using hydrogenic envelope functions [12] with Bohr radii calculated analytically or fitted variationally considering the anisotropic effective masses of Si. While Kettle *et al* [13] used EMT to study the effects of electric fields and interfaces non-perturbatively with a TCAD gate potential, this work ignored valley-orbit (VO) interaction responsible for lifting the degeneracies of the 1s manifold. A number of authors [14–16] used EMT to investigate the donor energy spectrum using symmetry arguments, perturbation theory, single or the multi-valley Schröedinger equation. In Ref [16], Friesen considered valley-orbit coupling and field effects in the effective mass formalism, to solve a multi-valley Schrödinger equation for the six 1s

states in the valley basis. Martins *et al* [17] used a TB sp^3s^* second nearest neighbor model to study effects of electric fields. In Ref [18] the BMB approach was proposed and applied to the same problem. Calderón *et al* [19] used EMT to investigate shuttling times of the donor electron between a donor-bound state and a surface bound state. Both TB and BMB approaches consider core effects and VO coupling explicitly to model impurities. The TB and the BMB methods are very different from each other in the sense that TB represents the Hamiltonian in real space while BMB represents it in momentum space. The close agreement of the results from two such different methods of calculations, as shown in this work, emphasizes the fundamental nature of the impurity physics. The work presented here resolves significant limitations of the previous treatments by including realistically large device components with over 3 million atoms in an atomistic treatment under realistic boundary conditions. This is also one of the first theoretical works on the Stark effect for P impurities to be benchmarked with a relevant experiment. While most theoretical approaches have concentrated on donor spectrum and wave functions near the ionization regime, little work has been done to explore the linear and quadratic Stark shifts of the hyperfine coupling far below the ionization regime for realistically large systems in the presence of interfaces.

The spin Hamiltonian of a donor electron in an applied electric field $\vec{\varepsilon}$ and a magnetic field $B_0\hat{z}$ is,

$$H_z = g(\vec{\varepsilon})\mu_B B_0 S_z + A(\vec{\varepsilon})I_z S_z \qquad (1)$$

where $A(\vec{\varepsilon})$ and $g(\vec{\varepsilon})$ are the hyperfine coupling constant and electron g-factor, respectively, as a function of electric field. The first term in the Hamiltonian is the spin-orbit Stark shift, while the second term is the hyperfine Stark shift. An electric field distorts the shape of the donor wave function, and modifies its angular momentum, which in turn modifies the g-factor. The field also pulls the donor wave function away from the impurity site, reducing $A(\vec{\varepsilon})$ which is proportional to $|\Psi(\vec{\varepsilon},\vec{r_0})|^2$, where $\vec{r_0}$ is the impurity site. The change in $A(\vec{\varepsilon})$ is parameterized as,

$$\Delta A(\vec{\varepsilon}) = A(0)(\eta_2\varepsilon^2 + \eta_1\varepsilon) \qquad (2)$$

The quadratic Stark coefficient η_2 was measured to be -3.7×10^{-3} $\mu m^2/V^2$ from the experiment by Bradbury *et al* [9]. The EMT result inferred from [16] in Ref [9] was -2×10^{-2} $\mu m^2/V^2$. Since the spin-orbit Stark effect is small for practical magnetic fields, this letter focuses on the behavior of $A(\vec{\varepsilon})$ only. An impurity placed far away from interfaces in an unstrained Si lattice experiences a dominant quadratic Stark effect for both $A(\vec{\varepsilon})$ and $g(\vec{\varepsilon})$. However, presence of nearby interfaces or lattice strain can produce a non-negligible linear Stark effect [20, 21].

The origin of the linear and quadratic Stark effects can be explained qualitatively from perturbation theory. The unperturbed ground state wave function for an impurity placed far away from interfaces has an approximate even symmetry. First order perturbation theory does not yield any energy correction if the perturbing Hamiltonian of a constant electric field is of odd symmetry. However, second order perturbation theory produces a quadratic dependence of the corrected energy on the field. If the impurity is very close to the interface, the even symmetry of the unperturbed wave function is broken. In such a case, first order perturbation theory also yields a linear dependence of the corrected energy on the electric field.

TB and BMB methods are separately used to calculate $A(\vec{\varepsilon})$. From each calculation, the ground state wave function $\Psi(\vec{\varepsilon},\vec{r})$ is calculated in the presence of the field $\vec{\varepsilon}$. The hyperfine coupling $A(\vec{\varepsilon})$ is determined by,

$$\frac{A(\vec{\varepsilon})}{A(0)} = \frac{|\Psi(\vec{\varepsilon},\vec{r_0})|^2}{|\Psi(0,\vec{r_0})|^2} \qquad (3)$$

In the range of low electric fields considered here, the excited states (E and T) are not expected to affect $A(\vec{\varepsilon})$ since this manifold is separated by 10 meV from the ground A_1 state. While EMT based approaches are concerned with contributions from valley-minima states only, TB and BMB approaches consider a more extensive Bloch structure of the material. TB and BMB also include valley-orbit (VO) interaction consistently, while most EMT treatments of VO are in violation of some of the assumptions made to derive the effective mass equation [18].

The BMB technique solves the Hamiltonian including an external electric field in a large but truncated basis of pure crystal Bloch states near the conduction band minima of a host obtained by the pseudo-potential method. Since the discretized Schrödinger equation is solved in reciprocal space, the Fourier transform of the impurity potential is used. Near the impurity core, the potential is modified from its Coulombic nature to include central cell effects. The corrected potential produces a broader Fourier spectrum in k-space and couples different valleys to lift the 1s degeneracies. The core potential in momentum (q) space used in [18] is,

$$U_{cor}(q) = \frac{1}{\pi^2\kappa}\left(\frac{\kappa\zeta q^2}{q^2+\alpha^2} + \frac{\kappa(1-\zeta)q^2}{q^2+\beta^2} - \frac{q^2}{q^2+\gamma^2}\right) \quad (4)$$

where κ is the dielectric constant of Si, assuming a value of $11.9\varepsilon_0$. The form and the parameters $(\zeta,\alpha,\beta,\gamma)$ of this potential have been taken from Pantelides [22]. An overall quenching factor provides a one-parameter fit to the ground state energy from which the excited state energies and degeneracies compare well with experiment. After inclusion of the external field the hyperfine coupling strength is obtained.

The standard technique in semi-empirical TB [23] is to optimize a parameter set to accurately reproduce the bulk band structure of a host. Once this is done, the

same set is used for atomistic modeling of any devices made of that host. For this work, the TB parameter set of $sp^3d^5s^*$ nearest-neighbor spin model for Si was optimized by genetic algorithm [24]. The donor potential used is,

$$V(\vec{r}) \;=\; \frac{e}{4\pi\kappa|\vec{r}-\vec{r_0}|}, \qquad \vec{r} \neq \vec{r_0} \qquad (5)$$

$$V(\vec{r}) \;=\; U_0, \qquad\qquad \vec{r} = \vec{r_0} \qquad (6)$$

The on-site core correcting potential U_0 is adjusted and found to be 4.33 eV to obtain the experimental ground state energy of 45.6 meV for Si:P. The potential due to the electric field is added to the diagonal of the Hamiltonian. The real space Hamiltonian with closed boundary conditions is solved by a parallel Lanczos algorithm in NEMO 3D [25] for the donor wave function.

Both methods described here are applicable to other hosts and impurities. To describe other Group V impurities, the hydrogenic coulomb potential is still valid in the bulk, but the core corrections need to be adjusted to reflect correct experimental binding energies.
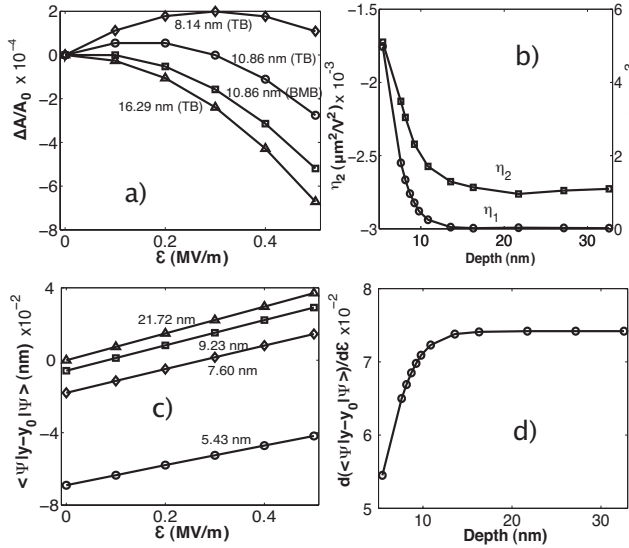

FIG. 1: (a) Electric field response of hyperfine coupling at various impurity depths (BMB and TB). (b) Quadratic (LH axis) and linear (RH axis) Stark coefficients with depth (TB). (c) Mean position of the ground state electron distribution (dipole moment) as a function of the electric field (TB). (d) The electric field gradient of the dipole moments (i.e. the slopes of the lines in (c)) with respect to depth (TB).

Fig. 1 summarizes the effects of the electric field and the interface on the donor electron. The TB calculations use a domain of 32 nm × 65 nm × 32 nm Zincblende lattice with 3.45 million atoms. The distance between the impurity and the interface is varied parallel to the electric field. The BMB calculation assumes a maximal depth of 10.86 nm from the interface, and employs a basis set of 7986 states. The choice of this depth is dictated by the ease of computation as it is sufficiently deep to nullify surface effects while not too deep to make the problem computationally intractable. In TB, a range of depths from 5 nm to 32 nm have been considered. For each TB data point, the typical computation times require about 7 hours on 20 CPUs [26]. Fig. 1(a) shows the variation of $\Delta A(\vec{\varepsilon})$ with electric field for various impurity depths. The data are fitted to the quadratic equation of (2) . As the depth increases, the quadratic coefficient η_2 approaches a constant value, while the linear coefficient η_1 becomes negligible (Fig. 1(b)). For small impurity depths, η_1 is comparable to η_2, which results in a shift of the peak of the parabola in Fig. 1(a) towards a non-zero electric field. If the linear Stark effect is negligible, an applied electric field has two effects on the ground state wave function: 1) a decrease in the peak amplitude of the wave function at the impurity site, reflected by a decrease in $A(\vec{\varepsilon})$ in Fig. 1(a) for higher depths, 2) a shift in the mean position of the wave function opposite the electric field, giving rise to a non-zero dipole moment as shown in Fig. 1(c). The dipole moments vary linearly with the electric field, and their slopes approach a constant value as the depth increases (Fig. 1(d)). The wave function plots of Fig. 2 also demonstrate these effects. The larger distortions of the wave function at higher electric fields explain the increasing dipole moments.
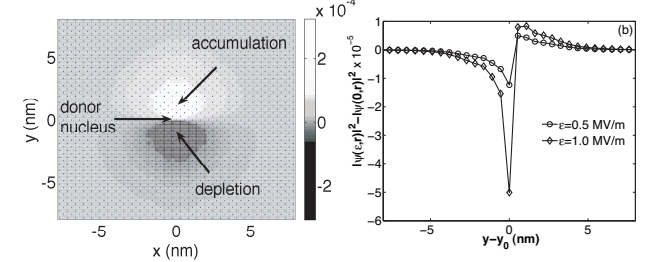

FIG. 2: (a) Electric field induced differential map of donor electron wave probability density, $|\Psi(\varepsilon, z_0)|^2 - |\Psi(0, z_0)|^2$, shown as a 2D cut through the impurity center at $z_0 = 16.29$ nm for $\varepsilon = 0.5$ MV/m. The electric field is directed along the negative y axis. (b) 1D cut though the center of the impurity parallel to the electric field showing the differential map of the probability density for two different electric fields.

If the impurity is close to the interface, the wave function is distorted even at zero electric field. This distortion comes from changes in the slope of the part of the wave function between the impurity and the interface. Also the mean position of the wavefunction shifts farther as the distance between the impurity and the interface is reduced. These effects give rise to an asymmetric charge distribution about the impurity, and a non-zero dipole moment is observed even at $\varepsilon = 0$. This is verified by the shift of the y-intercept of the lines in Fig. 1(c) for small impurity depths. In effect, the interface behaves like an electric field pushing the donor electron away from it. The strength of this field increases as the impurity is placed closer to the interface. This means that a higher electric field directed away from the interface is needed

TABLE I: Comparison of the quadratic Stark coefficients from experiment, EMT, BMB and TB.

Method	Depth (nm)	$\eta_2(\mu m^2/V^2)$
Experiment (Sb) [9]	150	-3.7×10^{-3}
EMT (P) [16]	∞	-2×10^{-2}
BMB (P)	10.86	-2.74×10^{-3}
TB (P)	10.86	-2.57×10^{-3}
	21.72	-2.76×10^{-3}

to counteract these interface effects and to restore the decreasing behavior of $A(\vec{\varepsilon})$, as demonstrated in Fig. 1(a).

Some of the numerical results can be explained qualitatively with the perturbation model using a basis of unperturbed impurity wave functions $\{\Psi_0^0, \Psi_1^0, ..., \Psi_m^0, ...\}$, where the superscript represents the order of correction and subscript the wave function index in order of decreasing binding energy (0 being the ground state). For an electric field Hamiltoninan given by $H = q\varepsilon y$, the wave function corrected to first order is expressed as,

$$|\Psi_0^1\rangle = |\Psi_0^0\rangle - q\varepsilon \sum_{m\neq0} \sum_i \frac{\langle\Psi_{m,i}^0|y|\Psi_0^0\rangle}{E_0^0 - E_{m,i}^0} \quad (7)$$

where i is the degeneracy index for a state m. The dipole moment $D = q\langle\Psi_0^1|y|\Psi_0^1\rangle$ is then given by,

$$D = q\langle\Psi_0^0|y|\Psi_0^0\rangle - 2q^2\varepsilon \sum_{m\neq0} \sum_i \frac{|\langle\Psi_{m,i}^0|y|\Psi_0^0\rangle|^2}{E_0^0 - E_{m,i}^0}$$
$$+ q^2\varepsilon^2 \sum_{m_{1,2}\neq0} \sum_{i,j} \frac{\langle\Psi_0^0|y|\Psi_{m_1,i}^0\rangle\langle\Psi_{m_2,j}^0|y|\Psi_0^0\rangle}{(E_0^0 - E_{m_1,i}^0)(E_0^0 - E_{m_2,j}^0)} (8)$$

The quadratic term in ε can be neglected compared to the other two terms for small ε. This results in a linear function with intercept and slope depending on $\langle\Psi_0^0|y|\Psi_0^0\rangle$ and $|\langle\Psi_0^0|y|\Psi_{m,i}^0\rangle|^2(E_0^0 - E_{m,i}^0)^{-1}$ respectively. For an impurity far away from the interface, the unperturbed ground state wave function is of even symmetry, and the expression for the intercept evaluates to zero. Since the unperturbed wave function symmetries and eigen-energies are not affected by depth any more, the expression for the slope assumes a constant value. On the other hand, for small impurity depths, the unperturbed wave functions get distorted depending on the depth. Since the ground state has no longer an even symmetry, the intercept evaluates to a non-zero quantity, in consistence with Fig. 1(c). The transition probabilities between the ground state and the excited states are also changed due to these distortions, causing the slope of the dipole moment to vary with depth, in consistence with Fig. 1(d). The same reasoning explains why the quadratic Stark coefficient approaches a constant value and the linear Stark coefficient becomes negligible with increasing depth.

Table 1 gives the comparison between theory and experiment and shows that the EMT estimate of η_2 differs by an order of magnitude, while TB and BMB estimates agree closely with each other and the experiment. The BMB estimate for a depth of 10.86 nm is already close to the converged TB estimate, although the peak $\Delta A(\vec{\varepsilon})$ at a non-zero ε in Fig. 1(a) indicates that the BMB estimate would improve even more at greater depths.

In summary, the Stark shift of the hyperfine coupling for Si:P in the presence of interfaces is analyzed from two very different theories (BMB and TB). The results of both methods are consistent and agree well with the experimental data for Si:Sb, thereby providing the most sensitive test of our understanding of shallow donor quantum control to date. For future work, both TB and BMB can be optimized for Sb donors, and the Stark shifts can be investigated in the presence of interfaces as well as lattice strain and a gate structure more closely resembling that of the experiment. In conclusion, we emphasize the need for very close interaction between theory and experiment to accomplish high precision control required in quantum computing.

Electronic address: rrahman@purdue.edu

[1] B. E. Kane, Nature, **393**, 133 (1998).
[2] R. Vrijen *et al.*, Phys. Rev. A **62**, 012306 (2000).
[3] C.D. Hill *et al.*, Phys. Rev. B **72**, 045350 (2005).
[4] R. deSousa *et al.*, Phys. Rev. A **70**, 052304 (2004).
[5] L. Hollenberg *et al.*, Phys. Rev. B **69**, 113301 (2004).
[6] L.C.L. Hollenberg *et al.*, Phys. Rev. B **74**, 045311 (2006).
[7] A. R. Stegner *et al.*, Nature Physics **2**, 835 (2006).
[8] Hans Huebl *et al.*, Phys. Rev. Lett. **97**, 166402 (2006).
[9] F. R. Bradbury *et al.*, Phys Rev. Lett. **97**, 176404 (2006).
[10] A. K. Ramdas *et al.*, Rep. Prog. Phys., Vol. **44** (1981).
[11] S. R. Schofield *et al.*, Phys. Rev. Lett. **91**, 136104 (2003).
[12] W. Kohn and J.M. Luttinger, Phys. Rev. **98**, 915 (1955).
[13] L. M. Kettle *et al.*, Phys. Rev. B **68**, 075317 (2003).
[14] A. Debernardi *et al.*, Phys. Rev. B **74**, 035202 (2006).
[15] G. D. J. Smit *et al.*, Phys. Rev. B **68**, 193302 (2003).
[16] M. Friesen, Phys. Rev. Lett. **94**, 186403 (2005).
[17] A. S. Martins*et al.*, Phys. Rev. B **69**, 085320 (2004).
[18] C. J. Wellard and L. C. L. Hollenberg, Phys. Rev. B **72**, 085202 (2005).
[19] M.J. Calderon *et al.*, Phys. Rev. Lett. **96**, 096802 (2006).
[20] G. M. Guichar *et al.*, Phys. Rev. B **5**, 422 (1972).
[21] D. K. Wilson and G. Feher, Phys. Rev. **124**, 1068 (1961).
[22] S. T. Pantelides and C.T. Sah, Phys. Rev. B **10**, 621 (1974).
[23] J. C. Slater and G.F. Koster, Phys. Rev. Vol. **94**, No. 6 (1954).
[24] T. B. Boykin *et al.*, Phys. Rev. B **69**, 115201 (2004).
[25] G. Klimeck *et al.*, CMES **3**, 601, (2002). The TB calculations have been done using the NEMO 3D tool.
[26] nanoHUB.org computational resource of a 256-node 3.3GHz Pentium Irvindale PC cluster was used.